Energy Distribution Curves of Ultrafast Laser-Induced Field Emission and Their Implications for Electron Dynamics

Hirofumi Yanagisawa,[1,*,†] Matthias Hengsberger,[1] Dominik Leuenberger,[1] Martin Klöckner,[1] Christian Hafner,[2] Thomas Greber,[1] and Jürg Osterwalder[1]

[1]*Physik Institut, Universität Zürich, Winterthurerstrasse 190, CH-8057 Zürich, Switzerland*

[2]*Laboratory for Electromagnetic Fields and Microwave Electronics, ETH Zürich, Gloriastrasse 35, CH-8092 Zürich, Switzerland*

(Received 22 March 2011; revised manuscript received 14 July 2011; published 16 August 2011)

Energy distribution curves of laser-induced electron pulses from a tungsten tip have been measured as a function of tip voltage and laser power. Electron emission via tunneling through and/or excitation over the surface barrier from photoexcited nonequilibrium electron distributions are clearly observed. The spectral shapes largely vary with the emission processes and are strongly affected by electron dynamics. Simulations successfully reproduce the spectra, thus allowing direct insight into the involved electron dynamics and revealing the temporal tunability of electron emission via the two experimental parameters. These results should be useful to optimize the pulse characteristics for many applications based on ultrafast laser-induced electron emission.

DOI: 10.1103/PhysRevLett.107.087601 PACS numbers: 79.70.+q, 78.47.J−, 79.60.−i, 79.90.+b

Applying strong electric fields to a metallic tip with nanometer sharpness enables electron emission via tunneling into the vacuum (field emission), producing continuous electron beams with high brightness and coherence [1–5]. Illumination of such tips by femtosecond laser pulses in combination with a moderate dc voltage applied to the tip has realized pulsed field emission with spatiotemporal control with femtosecond and nanometer resolution, making it attractive for both basic research and new applications like time-resolved electron microscopy, spectroscopy, holography, and also free-electron lasers [6–9]. However, the detailed spectral and temporal characteristics of such electron pulses with respect to variation of the relevant experimental parameters are as yet poorly known. Therefore, optimal conditions for their generation remain to be established.

So far, their emission mechanisms have been intensively studied [6–18]. It is reported that different processes become dominant depending on the strength of the optical fields on the tip apex [6,7,10,11,13]. For relatively weak fields, single-electron excitations by single- and multiphoton absorption are prevalent, and photoexcited electrons are tunneling through the surface potential barrier (photo-assisted field emission) or emitted over the barrier (photoemission). On the other hand, very strong fields largely modify the tunneling barrier and prompt field emission from the Fermi level (optical field emission).

Here, we used low-intensity laser pulses whereby electron dynamics due to strong-field effects are not supposed to be observed [17,18], and we characterize the laser-induced field emission from a tungsten tip spectrally and temporally by measuring electron energy distribution curves (EDCs) at high resolution, and by simulating transient EDCs for various laser powers and dc voltages. The results show spectral and temporal tunability via the two experimental parameters.

Figure 1(a) schematically illustrates our experimental setup. A tungsten tip with its axis along the [011] crystal direction is mounted inside a vacuum chamber (9×10^{-11} mbar). Laser pulses are generated in a Ti:sapphire oscillator (center wavelength: 800 nm; repetition rate: 76 MHz). The temporal spread of the laser-pulse intensity profile is estimated to be roughly 100 fs in FWHM just at the tip apex. The laser light was focused to 4 μm ($1/e^2$ radius) onto the tip apex. Linearly polarized laser light was used,

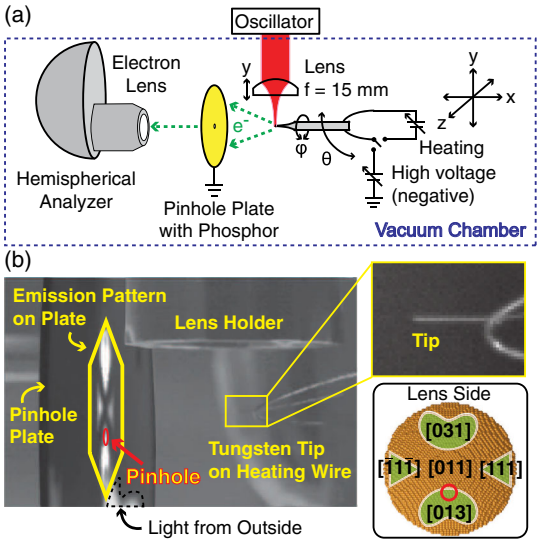

FIG. 1 (color online). (a) a schematic diagram of the experimental setup (see text for further description). (b) a photograph of the experimental setup. The inset is the front view of the atomic structure of the tip apex based on a ball model.

with the polarization vector parallel to the tip axis. The tip can be heated to clean the apex and also negatively biased for field emission. A pinhole plate with phosphor coating was mounted in front of the tip to observe emission patterns from the tip apex, and to define a specific emission site for electron spectroscopy. A hemispherical analyzer (VG: CLAM2) is used to measure EDCs of the emitted electrons passing through the pinhole. The tip can be moved along five axes as used in our previous work [7,8]. The tip axis is set to be orthogonal to the pinhole plate.

A photograph of the experimental setup is shown in Fig. 1(b). The field emission pattern of the clean tungsten tip can be observed on the phosphor plate where the most intense electron emission is observed around the [310]-type facets. The emission sites are highlighted by green (gray) areas with white edges on the schematic front view of the tip apex in the inset of Fig. 1(b). The pinhole is positioned at the edge of a [310] type facet, which is roughly indicated by a circle in the inset. Note that the selected site is also the most intense emission site in the laser-induced field emission [7,8].

Figure 2(a) shows an EDC of field emission at a tip voltage V_{tip} of -2300 V. The peak of the spectrum defines the Fermi energy E_F at 0 eV. The spectrum shows a typical asymmetric peak, which can be understood by the diagram in Fig. 2(a). The field emission current is influenced by two factors: (1) the electron occupation number and (2) the transmission probability through the surface barrier [1,2,19,20]. The occupation number is given by an electron distribution function $f(E)$, which is the Fermi-Dirac distribution function in the case of field emission, and the transmission probability depends exponentially on an area of the surface barrier indicated by the hatched area. Therefore, the positive energy side of the spectrum falls off due to a rapid decrease of the occupation number, while the negative energy side falls off because of the exponential decay of the transmission probability due to the increase of the surface barrier area. Thus a typical field emission spectrum shows such an asymmetric peak. An energy spread of 0.21 eV was observed, which is close to the value measured with 1 meV energy resolution in previous work (0.19 eV) [21], confirming our reasonable energy resolution.

Upon low-intensity laser irradiation, the electron distribution is modified by single-electron excitations due to multiphoton absorption, resulting in a nonequilibrium distribution characterized by a steplike profile as illustrated in the upper panel of Fig. 2(b) [15,22,23]; the width of each step corresponds to the photon energy $h\nu$ ($= 1.55$ eV). Here we identify the step edges of one-photon excitation (1PE), 2PE, and 3PE as shown in Fig. 2(b). In a real situation, however, the excited electrons relax mainly by electron-electron (e-e) scattering on a time scale of a few femtoseconds, which is shorter than our laser pulses. As a result, the electron dynamics is reflected in a smeared

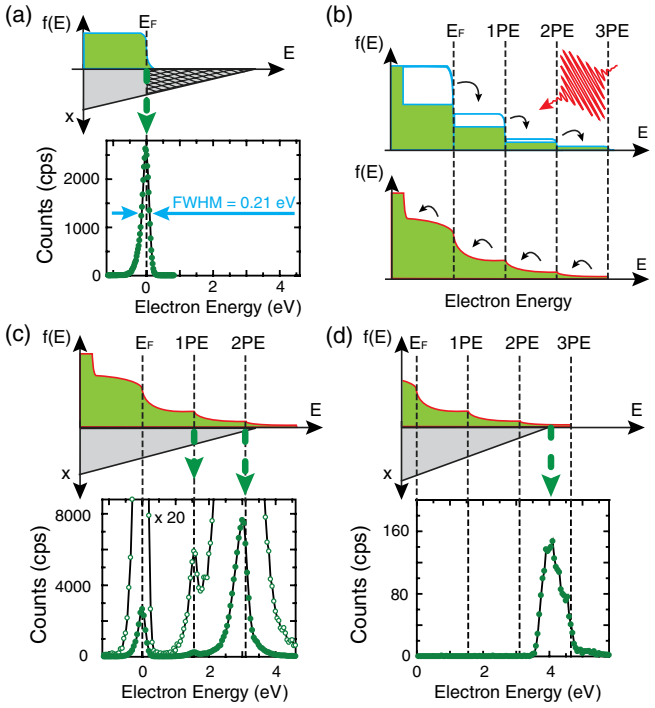

FIG. 2 (color online). (a) EDC of field emission from the tungsten tip together with a schematic diagram of field emission from a Fermi-Dirac distribution tunneling through a surface barrier. The transmission probability depends on the hatched area. The tip voltage V_{tip} was -2300 V. (b) schematic diagrams of nonequilibrium electron distributions just after laser absorption without (upper panel) and with (lower panel) electron-electron scattering. (c) and (d) show experimental EDCs and schematic diagrams of photoassisted field emission and photoemission, respectively. The magnified spectrum is also shown in (c). (c) $V_{\mathrm{tip}} = -2300$ V and the laser power $P_L = 50$ mW. (d) $V_{\mathrm{tip}} = -500$ V and $P_L = 50$ mW.

electron distribution, as shown in the lower panel of Fig. 2(b). This feature should be reflected in the EDCs.

Figure 2(c) shows an EDC of laser-induced field emission at $V_{\mathrm{tip}} = -2300$ V and a laser power P_L of 50 mW. The spectrum shows the field emission peak undisturbed with identical shape and intensity as in Fig. 2(a), and additional peaks at the 1PE and 2PE edges are clearly observed. The latter show the same asymmetric shape as the field emission peak. Thus, photoassisted field emission is confirmed experimentally. Regarding the relative intensities, photoassisted field emission from 2PE is much higher than that from 1PE even though the occupation number at 1PE is higher; this is because the transmission probability at 2PE is quite high. Note that photoassisted field emission from 2PE has not been observed for excitation with a continuous-wave laser [24]; these electron distributions are supposed to be largely different from our case.

An EDC at $V_{\mathrm{tip}} = -500$ V and $P_L = 50$ mW is displayed in Fig. 2(d). In this spectrum, the nonequilibrium

electron distribution function becomes more noticeable. Field emission and photoassisted field emission processes are suppressed due to the low dc field, and photoemission over the surface barrier dominates, for which 3PE is required. The peak shows a spectral shape completely different from that of field emission. The peak maximum is located at approximately 0.65 eV below the 3PE edge. Since the transmission probability is unity throughout the photoemission regime, the peak shape reflects more closely the electron distribution function. Therefore the spectral shape indicates a strong modulation of the electron distribution due to *e-e* scattering processes.

Further investigations of the spectral shapes were done by systematically measuring EDCs for various tip voltages and laser powers as shown in Fig. 3. These spectra show a smooth parametric transition between field emission, photoassisted field emission and photoemission. As a rule of thumb, with decreasing tip voltage and increasing laser power, the photoemission process becomes dominant, which is consistent with previous work [8,12,13]. Throughout the whole range of experimental parameters, no clear onset of optical field emission is observed, which would be characterized by reentrant strong emission at E_F. The inset of Fig. 3 shows a characteristic increase of intensities as a function of laser power for each excitation order at $V_{\text{tip}} = -2300$ V. The field emission (FE) intensity remains constant.

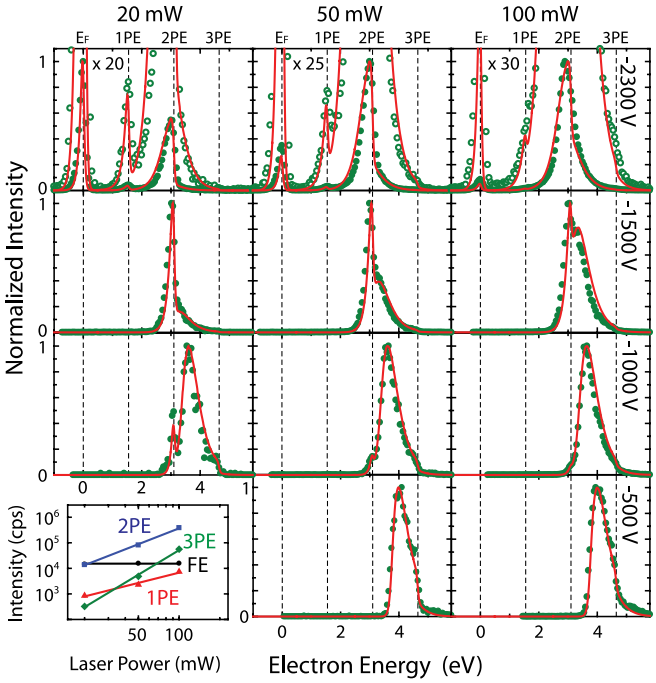

FIG. 3 (color online). Measured and simulated EDCs for different tip voltages (dc fields F_{dc}) and laser powers [excitation constant C_{exc}, appears in Eq. (1)]. The work function Φ of 4.592 eV was used for the simulation. All the spectra are normalized at their maximum values. The measured EDCs are shown as dots, and the simulated EDCs as lines. Magnified spectra are also shown in the spectra at $V_{\text{tip}} = -2300$ V as circles for the experiments and lines for the simulations. The inset (bottom left) shows the measured laser power dependence of intensities for each excitation order ($V_{\text{tip}} = -2300$ V). These intensities were obtained by integrating intensities over the respective energy regions: field emission (FE) is for -1.2–0.3 eV, photoassisted field emission and photoemission from 1PE for 0.3–1.85 eV, 2PE for 1.85–3.4 eV and 3PE for 3.4–4.95 eV. The lines are fitting curves with power functions; exponents are 1.3, 2.1, and 3.2 for 1PE, 2PE, and 3PE, respectively.

The influence of electron dynamics in the emission was clarified by simulating transient EDCs. The basic approach was the same as that used in Refs. [15,23,25,26]. *e-e* interaction, electron-phonon (*e-p*) interaction, and single-electron excitation by single-photon absorption are included in a system of Boltzmann's equations to obtain the temporal evolution of the distribution function of the electron gas and the phonon gas. Fermi-Dirac and Bose-Einstein distributions at room temperature were assumed as initial conditions. The collision terms that describe *e-e* and *e-p* scattering were given in Refs. [23,25], and the term for the electron-gas excitation by the pump pulse was given in Ref. [26] as

$$H(E,t) = C_{\text{exc}} F(t)_{\text{gauss}} \{\sqrt{E-\hbar\nu} f(E-\hbar\nu)[1-f(E)] - \sqrt{E+\hbar\nu} f(E)[1-f(E+\hbar\nu)]\}, \quad (1)$$

where $F(t)_{\text{gauss}}$ is a Gaussian function with a maximum of unity and a temporal spread of 100 fs in FWHM, and C_{exc} is an excitation constant which is proportional to the laser power and is used as a fitting parameter in our simulations. To calculate *e-e* and *e-p* scattering, we used free-electron and Debye models with a Fermi energy of 9.2 eV [27], a Debye temperature of 400 K [28], and a sound speed for longitudinal phonons of 5220 m/s [29]. Calculation of EDCs were done by using the Fowler-Nordheim theory, as in previous work [7,8,15].

In the simulations, a laser pulse is moved in 0.2 fs steps from -200 to 1200 fs across the emission site, where the time zero is defined when the pulse maximum meets the emission site as shown in the schematic diagram of Fig. 4(a). Note that the time steps were refined until convergence was reached at 0.2 fs. Electron distribution functions and EDCs were calculated at each time step. The resulting transient EDCs were integrated over the entire time interval. EDCs of field emission without laser excitation were also calculated for the rest of one period of the laser-pulse repetition cycle (approximately 10 ns), and added to the EDCs from the first 1400 fs; the resulting time-integrated EDCs were normalized at the maximum intensity. Thus obtained simulations were compared with the measured EDCs normalized at their maximum intensities. Quantitative comparisons based on the absolute intensities were not done because the transmission function of the spectrometer is not well known. There are only three

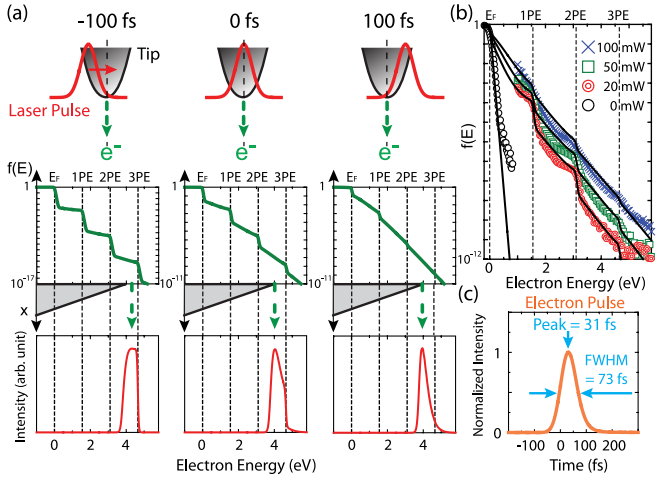

FIG. 4 (color online). (a) Schematic diagrams and examples of simulations at three time steps. Transient electron distribution functions (upper) and EDCs (lower) are shown. The three EDCs are not drawn to scale. The following fitting parameters were used: $F_{\mathrm{dc}} = 0.502$ V/nm, $C_{\mathrm{exc}} = 4.25 \times 10^{-5}$, $\Phi = 4.592$ eV. (b) Fermi-Dirac and time-averaged transient electron distribution extracted from field emission and photoassisted field emission spectra at $V_{\mathrm{tip}} = -2300$ V together with corresponding simulation curves (solid lines). The extracted data were normalized to be 0.5 at 0 eV and then multiplied by (laser-pulse cycle)/(simulation period). The data points below 1 eV were cut to show only transient electron distribution. (c) Temporal line profile of the simulated electron pulse.

fitting parameters: (1) the work function Φ, (2) the dc field F_{dc}, and (3) the excitation constant C_{exc}. Fitting was done first by adjusting these three parameters at one particular setting of the tip voltage and laser power ($V_{\mathrm{tip}} = -500$ V; $P_L = 50$ mW), and then by simulating time-integrated EDCs for the other settings by scaling up or down F_{dc} and C_{exc} according to the corresponding tip voltage and laser power. This procedure was iterated until reasonable fitting was obtained for all settings.

Figure 4(a) shows simulations at three time steps. The electron distribution at -100 fs shows a clear multiple step character, but due to the scattering processes the distribution function becomes more and more smeared out as time goes on. Accordingly, the transient EDCs change their shapes and peak positions with time, showing a relaxation of photoexcited electrons to lower energies. The resulting time-integrated EDCs are in good agreement with the corresponding experimental EDCs as shown in Fig. 3 at $V_{\mathrm{tip}} = -500$ V and $P_L = 50$ mW. The obtained fitting parameters of $F_{\mathrm{dc}} = 0.502$ V/nm and $C_{\mathrm{exc}} = 4.25 \times 10^{-5}$ at this setting were scaled up or down according to the other settings of V_{tip} and P_L in Fig. 3. Then the time-integrated EDCs were calculated for all the other experimental EDCs. Throughout all the various conditions, the simulations are in very good accordance with the experimental EDCs. Thus we conclude that electron dynamics play a significant role in the electron emission. In fact, time-averaged nonequilibrium electron distribution functions can be extracted by normalizing the experimental EDCs by the expected tunneling probabilities as shown in Fig. 4(b). The extracted data are in good agreement with the simulated curves for all laser powers. The steps become more and more smeared out with increasing laser power because more excited electrons can scatter into lower energy states, an effect which was also discussed in a previous study [11,12].

Based on the successful modeling, we further calculate temporal profiles of electron pulses and comment on the relevance of these findings in view of designing pulsed electron sources for the applications mentioned earlier. From the quantitative description of experimental EDCs achieved with our simulations, we can be confident to predict the temporal characteristics of electron pulses from the energy-integrated transient EDCs; an example result for $V_{\mathrm{tip}} = -500$ V and $P_L = 50$ mW is shown in Fig. 4(c). The profile shows a delay of peak emission (31 fs) and a squeeze of temporal width (73 fs) relative to the laser pulse. The delay is caused by the electron dynamics. The squeeze is due to the nonlinearity of the multiphoton excitations. As a rule of thumb, these values as well as energy spreads increase with laser power, before even considering space charge effects in the vacuum [30]. Such an increase is not desirable for applications in general. On the other hand, the electron emission current increases with laser power. To reach higher intensities while keeping energy and temporal spreads low, photoassisted field emission from a tip array [16,31] illuminated by low-power laser pulses is considered to be the optimal solution. Single tip sources used in time-resolved electron microscopy or holography could potentially reveal dynamical properties of nanoobjects.

This work was supported by the Swiss National Science Foundation through the Ambizione (Grant No. PZ00P2_131701) and the NCCR MUST. We thank Professor H. W. Fink for discussions.

*Present address: Department of Physics, ETH Zürich, Wolfgang-Pauli-Strasse 16, CH-8093 Zürich, Swizerland.
†hirofumi@phys.ethz.ch

[1] R. Gomer, *Field Emission and Field Ionization* (American Institute of Physics, New York, 1993).
[2] G. Fursey, *Field Emission in Vacuum Microelectronics* (Kluwer Academic/Plenum Publishers, New York, 2003).
[3] H. W. Fink, IBM J. Res. Dev. **30**, 460 (1986).
[4] K. Nagaoka *et al.*, Nature (London) **396**, 557 (1998).
[5] B. Cho *et al.*, Phys. Rev. Lett. **92**, 246103 (2004).
[6] P. Hommelhoff *et al.*, Phys. Rev. Lett. **96**, 077401 (2006).
[7] H. Yanagisawa *et al.*, Phys. Rev. Lett. **103**, 257603 (2009).
[8] H. Yanagisawa *et al.*, Phys. Rev. B **81**, 115429 (2010).
[9] M. Aeschlimann *et al.*, Nature (London) **446**, 301 (2007).

[10] P. Hommelhoff, C. Kealhofer, and M. A. Kasevich, Phys. Rev. Lett. **97**, 247402 (2006).
[11] C. Ropers *et al.*, Phys. Rev. Lett. **98**, 043907 (2007).
[12] C. Ropers *et al.*, New J. Phys. **9**, 397 (2007).
[13] B. Barwick *et al.*, New J. Phys. **9**, 142 (2007).
[14] R. Ganter *et al.*, Phys. Rev. Lett. **100**, 064801 (2008).
[15] L. Wu and L. K. Ang, Phys. Rev. B **78**, 224112 (2008).
[16] S. Tujino *et al.*, Appl. Phys. Lett. **94**, 093508 (2009).
[17] R. Bormann *et al.*, Phys. Rev. Lett. **105**, 147601 (2010).
[18] M. Schenk, M. Kruger, and P. Hommelhoff, Phys. Rev. Lett. **105**, 257601 (2010).
[19] E. L. Murphy *et al.*, Phys. Rev. **102**, 1464 (1956).
[20] R. D. Young, Phys. Rev. **113**, 110 (1959).
[21] H. Ogawa *et al.*, Surf. Sci. **357–358**, 371 (1996).
[22] M. Lisowski *et al.*, Appl. Phys. A **78**, 165 (2004).
[23] B. Rethfeld *et al.*, Phys. Rev. B **65**, 214303 (2002).
[24] Y. Gao and R. Reifenberger, Phys. Rev. B **32**, 1380 (1985).
[25] B. Rethfeld, Ph.D. thesis, Technische Universität Braunschweig, 1999.
[26] N. Del Fatti *et al.*, Phys. Rev. B **61**, 16 956 (2000).
[27] M. F. Islam *et al.*, Solid State Commun. **149**, 1257 (2009).
[28] C. Kittel, *Introduction to Solid State Physics* (John Wiley & Sons, New York, 2005), 8th ed.
[29] *CRC Handbook of Chemistry and Physics*, edited by D. R. Lide (CRC Press, Boca Raton, FL, 2009), 90th ed.
[30] See Supplemental Material at http://link.aps.org/supplemental/10.1103/PhysRevLett.107.087601 for a table showing four characteristic parameters of electron pulses for various tip voltages and laser powers: (I) Energy spread, (II) temporal spread, (III) delay of the electron pulse with respect to the laser pulse, and (IV) the number of emitted electrons per pulse.
[31] E. Kirk *et al.*, J. Vac. Sci. Technol. B **27**, 1813 (2009).